ResearchGate

See discussions, stats, and author profiles for this publication at: https://www.researchgate.net/publication/265736936

First-Principles Study of Water Reaction and H2 Formation on UO2 (111) and (110) Single Crystal Surfaces

ARTICLE *in* THE JOURNAL OF PHYSICAL CHEMISTRY C · SEPTEMBER 2014

Impact Factor: 4.77 · DOI: 10.1021/jp503614f

CITATIONS
3

READS
25

8 AUTHORS, INCLUDING:

Jian Hui Lan
Chinese Academy of Sciences
53 PUBLICATIONS **1,419** CITATIONS
SEE PROFILE

Wei-Qun Shi
Chinese Academy of Sciences
70 PUBLICATIONS **502** CITATIONS
SEE PROFILE

Available from: Jian Hui Lan
Retrieved on: 03 February 2016

THE JOURNAL OF PHYSICAL CHEMISTRY C

Article

pubs.acs.org/JPCC

First-Principles Study of Water Reaction and H_2 Formation on UO_2 (111) and (110) Single Crystal Surfaces

Tao Bo,[†,‡] Jian-Hui Lan,[†] Cong-Zhi Wang,[†] Yao-Lin Zhao,[‡] Chao-Hui He,[‡] Yu-Juan Zhang,[†] Zhi-Fang Chai,*[,†,§] and Wei-Qun Shi*[,†]

[†]Key Laboratory of Nuclear Radiation and Nuclear Energy Technology and Key Laboratory for Biomedical Effects of Nanomaterials and Nanosafety, Institute of High Energy Physics, Chinese Academy of Sciences, Beijing 100049, China

[‡]School of Nuclear Science and Technology, Xi'an Jiaotong University, Xi'an 710049, China

[§]School for Radiological and Interdisciplinary Sciences (RAD-X) and Collaborative Innovation Center of Radiation Medicine of Jiangsu Higher Education Institutions, Soochow University, Suzhou 215123, China

Supporting Information

ABSTRACT: Molecular and dissociative adsorption behavior of H_2O along with the accompanying H_2 formation mechanism on the UO_2 (111) and (110) surfaces have been investigated by using DFT+U calculations. According to our calculations, the higher stability of the (111) surface leads to higher oxygen vacancy formation energy compared to the (110) surface. On the stoichiometric (111) and (110) surfaces, the first hydrogen atom of water molecule can dissociate readily with very small or no energy barrier. On the contrary, dissociation of the second one becomes the rate-determining step, and water-catalysis leads to the decrease of energy barrier from 0.92 to 0.70 eV and from 2.36 to 1.21 eV on the stoichiometric (111) and (110) surfaces, respectively. H_2 formation resulting from water dissociation may undergo two pathways in the presence of surface oxygen vacancy on the reduced UO_2 (111) surface. One is characterized by direct combination of two hydrogen atoms of one water molecule, and the other is characterized by dissociation of the first hydrogen atom and its combination with a neighboring surface hydrogen atom. The above two formation pathways possess the energy barriers of 0.56 and 0.53 eV, corresponding to the large reaction energies of −2.62 and −2.64 eV, respectively.

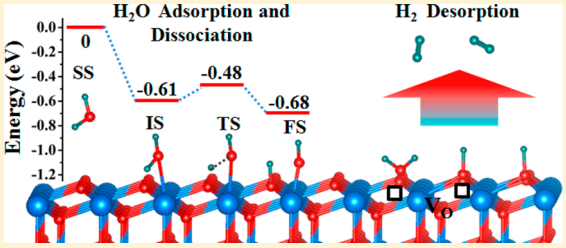

1. INTRODUCTION

The scientific study of actinide compounds is of great interest due to their large demand in the nuclear energy industry and for environmental preservation and long-term storage of radioactive waste.[1,2] However, surface actinide chemistry has been rarely concerned owing to the chemical complexity and radioactivity of 5f-block solid material to date.[3] At present, a thorough understanding of surface properties of actinide compounds is urgently required actually because surface problems can be confronted in each field concerning actinide compounds, especially in surface protection[4] and long-term storage of radioactive waste.[1] Surface corrosion generally results from the gas/liquid−solid interface interaction with media from the environment such as oxygen and water, and the interface behavior of adsorbates on actinide surfaces is an essential scientific issue.

In the past decades, people found that it is difficult to fully reveal the complex chemical properties of actinides due to the complex electronic structure properties of 5f states.[5] To reasonably estimate the strong on-site Coulomb repulsion of 5f electrons, the DFT+U method has been applied to study actinide compounds and related surface problems.[6−10] For example, Boettger et al.[11] have studied the clean and hydroxylated UO_2 (111), PuO_2 (111), and NpO_2 (111) surfaces within the generalized gradient approximation (GGA) to DFT. In this work, UO_2 was incorrectly predicted to be metal instead of insulator. Skomurski et al.[12] have studied the potential reactivity and relaxation mechanisms of UO_2 (111), (110), and (100) surfaces by using DFT and empirical potential computational methods. In another study, Skomurski et al.[4] have studied the adsorption of a single water molecule on the UO_2 (111) and ThO_2 (111) surfaces by using DFT method. Alexandrov et al.[13] have studied the surface energies and adsorption enthalpies of water on ThO_2 surfaces by combining accurate calorimetric measurements and first-principles studies. In this work, the coverage-dependent adsorption enthalpies and a mixed molecular and dissociative adsorption structure for the first hydration layer were determined. Rák et al.[8] have investigated the dissociative adsorption of water on UO_2, PuO_2, and NpO_2 surfaces by using the DFT+U method, in which both the bulk UO_2 and UO_2 surface slabs were correctly predicted to be insulators. Jomard et al.[14] have studied the thermodynamic stability of various terminations of PuO_2 (111), (110), and (100) surfaces by using PBE and PBE+U methods.

Received: April 13, 2014
Revised: September 3, 2014
Published: September 3, 2014

ACS Publications © 2014 American Chemical Society

In their work, the PBE calculations predicted an unexpected stabilization of O_2-(111) and Pu-(111) terminations under very low or extremely high temperatures, while the PBE+U calculations predicted the unique stabilized O-(111) termination over the entire temperature range, regardless of oxygen partial pressure. Sun et al.[15] have systematically studied the surface properties of PuO_2 (111), (110), and (100) surfaces and the effect of O-vacancy with various concentrations upon the surface stability by using GGA+U calculation and ab initio atomistic thermodynamics method. They concluded that under different oxygen environment the stoichiometric and reduced PuO_2 surfaces have different stability. Maldonado et al.[9] have computed the pressure−temperature phase diagrams of water adsorption reactions on UO_2 (111), (211), and (221) surfaces by using the DFT+U method in combination with atomistic thermodynamic simulations. They found that the (111) surface is less favorable for water adsorption than the other two surfaces, and the most favorable water coverage on the (111) surface is either 0.5 or 0.25 ML depending on the temperature and water partial pressure. In experiment, Senanayake et al.[16] studied water reaction with the stoichiometric and reduced UO_2 (111) surface and observed the phenomenon of H_2 desorption during the TPD study.

Among actinide compounds, uranium dioxide is the most commonly used fuel in the nuclear reactors operating today, meaning that UO_2 is the main component of spent nuclear fuel around the world. The reactions of uranium dioxide with water affect a variety of processes in the nuclear fuel cycle ranging from fabrication of nuclear fuels to spent fuel storage in water and direct disposal of spent fuels in a deep geologic repository.[1] In addition, it is associated with many fundamental phenomena related to hydrogen production,[17,18] corrosion,[4] and modifications of crystal morphologies.[19,20] However, based on the above discussion, the application of the DFT+U method to solve surface problems of uranium dioxide is rarely reported. In any case, a systematic study of water reaction with UO_2 surfaces is urgently required to better understand the UO_2−water interfacial interactions.

In this work, we intend to use DFT-based electronic structure methods to elucidate: (1) the reaction properties of water molecule with the stoichiometric and reduced UO_2 (111) and (110) surfaces and (2) the formation mechanism of H_2 molecule following water dissociation on the reduced UO_2 (111) surface. This paper is organized as below. First, we examine the basic physichemical properties of stoichiometric and reduced (111) and (110) surfaces. Second, the molecular and dissociative adsorption behaviors of water on the stoichiometric and reduced (111) and (110) surfaces are discussed in detail. Finally, we illustrate the formation and desorption mechanisms of H_2 on the reduced (111) surface. This work can shed light on the understanding of interface interaction of water with actinide oxides.

2. COMPUTATIONAL METHODOLOGY

All calculations were performed by using the plane wave density functional theory implemented in the Vienna ab initio simulation package (VASP).[21−23] The projector augmented wave (PAW)[24,25] method was used to describe the electron−ion interaction. The electron exchange correlation energy was calculated within the generalized gradient approximation in the Perdew−Burke−Ernzerhof formalism (GGA-PBE).[26] A plane-wave cutoff of 510 eV and the Gaussian electron smearing method with σ = 0.20 eV were used in all the calculations to ensure the convergence of the total energy within 3 meV per unit cell. Spin-polarization was included in all the structural optimizations. The Brillouin zone integration was calculated using 4 × 4 × 4 and 3 × 3 × 1 Monkhorst−Pack k-point meshs[27] for the UO_2 bulk and surfaces, respectively. Geometric relaxation was obtained with the quasi-Newton (variable metric) algorithm until the forces on all the atoms were smaller than 0.02 eV/Å. After the equilibrium lattice constants were determined, the shape and volume of the adopted slabs keep unchanged.

The UO_2 surface models were built on the basis of the UO_2 bulk with the calculated lattice constant of a = 5.544 Å, which agrees well with the experimental value of 5.47 Å[28] and previous theoretical work.[8] The UO_2 surfaces were modeled by periodic $p(2 \times 2)$ slabs, which consist of nine and six atomic monolayers (MLs) for (111) and (110) surfaces, respectively. A vacuum spacing was set as 15 Å along the surface normal directions to minimize the interaction between successive slabs in all the surface models. Convergence tests were performed to make sure that the results were well converged with respects to these parameters. Since DFT could not properly handle the strong on-site Coulomb repulsion of 5f electrons, a Hubbard term with U = 4 eV was added to ensure the insulating property of uranium dioxide. In this work, the symmetry was canceled in order to avoid the frequently encountered metastable structures during optimizations. Given the complications resulting from the antiferromagnetic (AFM) ordering of magnetic moments, we used the ferromagnetic (FM) configuration in all the first-principles calculations. Previous literature[29,30] indicates that the difference in the total energies of the FM and AFM configurations was about tens of meV.

There are many possible reactive sites for water adsorption on stoichiometric and reduced UO_2 surfaces, considering the diversity of orientation of water molecule and its dissociation products. To probe all the possible adsorption sites, a series of ab initio molecular dynamics (AIMD) simulations[9,13] were performed within the NVT ensemble. These AIMD simulations were carried out at a temperature of 300 K starting with different initial atomic configurations of water molecule and ran up to 10 ps with a time step of 1 fs. In the AIMD simulations the cutoff energy was set to 250 eV while the mesh k-points grid was restricted to the Γ-point. The lowest energy structures obtained by the AIMD simulations were all optimized by DFT +U methods again.

The surface energy E_{surf} is defined as

$$E_{surf} = \frac{1}{2A}(E^N_{slab} - NE_{bulk}) \quad (1)$$

where E^N_{slab} is the total energy of the slab containing N formula-unit, E_{bulk} denotes the total energy of one formula-unit of the bulk reference system. The formation energy of oxygen vacancy is defined as

$$E_{for} = E(\text{r-slab}) + 1/2E(O_2) - E(\text{s-slab}) \quad (2)$$

where E(r-slab) and E(s-slab) are the total energies of the reduced and stoichiometric slabs, respectively; $E(O_2)$ is the total energy of a free oxygen molecule. The adsorption energy, E_{ad}, can thus be calculated as

$$E_{ad} = E(\text{adsorbate/slab}) - E(\text{slab}) - E(\text{adsorbate}) \quad (3)$$

where E(adsorbate/slab) is the total energy of the uranium dioxide slab with the adsorbed adsorbate molecule; E(slab) and E(adsorbate) are the total energies of the slab and free

dx.doi.org/10.1021/jp503614f | J. Phys. Chem. C 2014, 118, 21935−21944

adsorbate molecule, respectively. The reaction paths including transition states and activation barriers were obtained by using the climbing image nudge elastic band (CI-NEB) method.[31−33] Four images were used for these calculations.

3. RESULTS AND DISCUSSION

3.1. Properties of Stoichiometric and Reduced (111) and (110) Surfaces. Uranium dioxide possesses a cubic fluorite structure with eight oxygen neighbors for each uranium ion. In this section, we aim to discuss the thermodynamic stability of two low index oxygen-terminated surfaces of uranium dioxide, that is, (111) and (110). Figure 1a,b shows the slabs adopted to model the studied stoichiometric and reduced UO_2 surfaces. The slabs were built on the basis of a relaxed UO_2 bulk unit cell with the calculated lattice constant of a = 5.544 Å. The relative stability of low index UO_2 surfaces was discussed according to the obtained surface energies. As

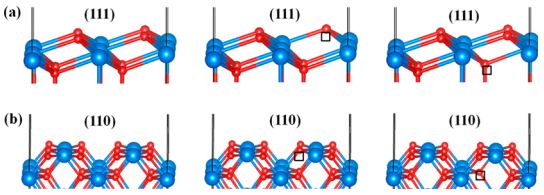

Figure 1. Models of stoichiometric and reduced (a) (111) and (b) (110) surfaces of UO_2 crystal. The left, middle, and right columns represent the stoichiometric surfaces, reduced surfaces with a first layer oxygen vacancy, and a second layer oxygen vacancy, respectively. The oxygen and uranium atoms are plotted in red and blue, respectively. The black boxes denote oxygen vacancies.

Table 1. Surface Energies and Formation Energies of Oxygen Vacancy in the First and Second Layers of the (111) and (110) Surfaces of UO_2

		formation energy	
	surface energy (J/m^2)	first layer (eV)	second layer (eV)
(111)	0.73	5.95	6.08
(110)	1.06	5.38	5.59

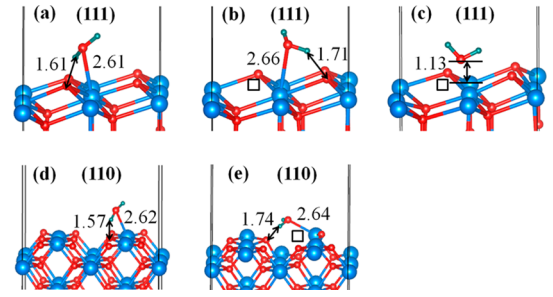

Figure 3. Optimized adsorption structures of water monomer on the (a, d) stoichiometric and (b, c, and e) reduced (111) and (110) surfaces of UO_2 crystal. The oxygen and hydrogen atoms are plotted in red and green, respectively, while the uranium atoms are blue. The black boxes denote oxygen vacancies. The distance unit is Å.

Table 2. Adsorption Energies of Molecular and Dissociative Water Located on the Stoichiometric and Reduced UO_2 (111) and (110) Surfaces

	(111)		(110)	
state of water	stoich.	redu.	stoich.	redu.
molecule	−0.61	−0.94/−0.88	−0.62	−1.42
partial dissociation[a]	−0.68	−2.20	−1.27	−1.78/−2.11
complete dissociation[a]	0.15		−0.11	

[a]Partical and complete dissociation denotes the broken of one and two O−H bonds of water molecule, respectively. The energy unit is eV.

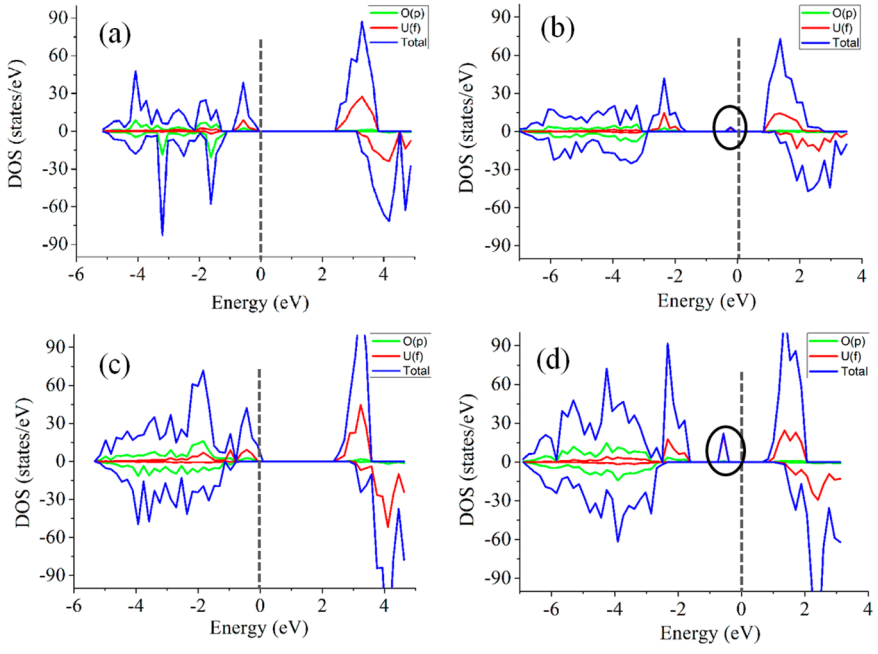

Figure 2. Total and projected density of states (DOS) for the stoichiometric (111) surface (a), reduced (111) surface (b), stoichiometric (110) surface (c), and reduced (110) surface (d). Here the oxygen vacancy exists in the first oxygen layer of two reduced surfaces. The blue line represents the total DOS of the slabs, while green and red lines represent the projected DOS for O-2p and U-5f orbitals of the first surface layer of UO_2 surfaces. Fermi energy is set as zero and marked by the vertical dashed line.

dx.doi.org/10.1021/jp503614f | J. Phys. Chem. C 2014, 118, 21935−21944

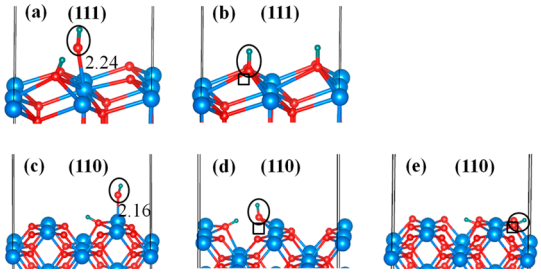

Figure 4. Optimized structures for partially dissociative adsorption of water on the (a, c) stoichiometric and (b, d, and e) reduced (111) and (110) surfaces of UO_2 crystal. The black boxes denote oxygen vacancies, and the circles denote hydroxyl radicals from water dissociation. The distance unit is Å. Color code as in Figure 3.

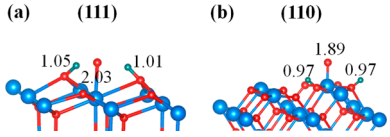

Figure 5. Optimized adsorption structures with complete water dissociation on the stoichiometric UO_2 (111) (a) and (110) (b) surfaces, respectively. The distance unit is Å. Color code as in Figure 3.

shown in Table 1, the calculated surface energies for the (111) and (110) surfaces are 0.73 and 1.06 J/m^2, respectively. These values agree very well with previous first-principles investigation,[8] in which these surface energies were calculated to be 0.78, and 1.05 J/m^2, respectively. From the above results, the UO_2 (111) surface becomes more stable than the (110) case, and the surface stability conforms to the following order: (111) > (110).

As is well-known, the oxygen vacancy formed by losing a single oxygen atom is the most popular intrinsic defect in UO_2. Here, we compared the formation energy of oxygen vacancy in bulk UO_2 and on the (111) and (110) surfaces. In bulk UO_2, the formation energy was calculated to be about 6.14 eV by using a $p(2 \times 2 \times 2)$ supercell. For UO_2 surfaces, we considered removing a single oxygen atom from both the top two oxygen layers as shown in Figure 1. In Table 1, the formation energies of oxygen vacancy in the first oxygen layer were calculated to be 5.95 and 5.38 eV for the (111) and (110) surfaces, respectively. As expected, these values are lower than the bulk values which support the idea that these low index UO_2 surfaces are more reactive than the bulk. For oxygen vacancy in the second oxygen layer, the formation energies for the (111) and (110) surfaces were calculated to be 6.08 and 5.59 eV, respectively. These values are a bit larger than those for the first oxygen layer, indicating that the second oxygen layer preserves more bulk characteristics than the first oxygen layer of the studied UO_2 slabs. In addition, the more stable (111) surface has higher oxygen vacancy formation energy.

Figure 2 shows the spin-polarized total and projected density of states (TDOS and PDOS) of stoichiometric and reduced UO_2 (111) and (110) surfaces. For comparison, we presented the PDOS for O 2p and U 5f orbitals of the first surface layer of these two surfaces, which predominates the surface activity and spectral characteristics of UO_2 around the Fermi energy. As shown in Figure 2a,c, for stoichiometric surfaces, each system has a band gap value of about 2.3 eV, which is comparable to the experimental value of 2.1 eV.[3] According to our previous investigations on bulk UO_2,[6] the top two separate valence

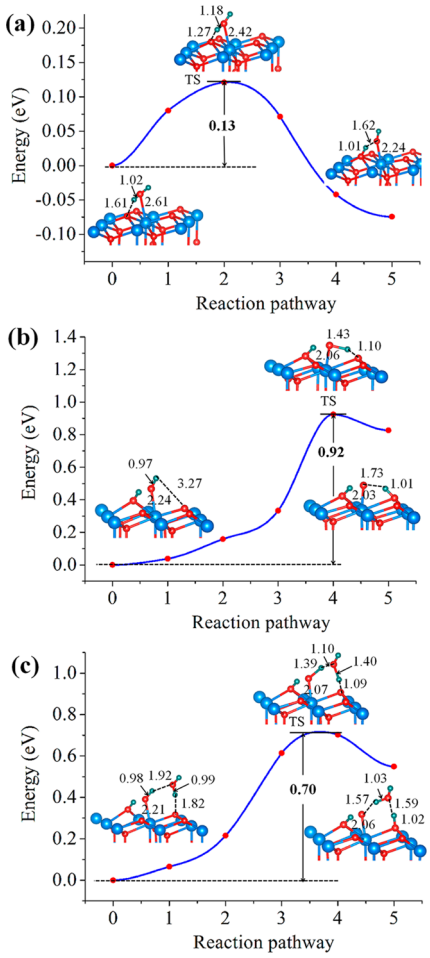

Figure 6. Calculated energy profiles for water dissociation: (a) first dehydrogenation, (b) second dehydrogenation, and (c) second dehydrogenation catalyzed by water molecule on the stoichiometric (111) surface. The insets correspond to the optimized structures of the initial state (left), transition state (middle), and final state (right). The distance unit is Å. Color code as in Figure 3.

bands below the Fermi energy correspond to the U−O bonding (wide band) and the localized unpaired U 5f orbitals (narrow band), respectively. However, an unexpected observation from the surface TDOS is that the small gap between the top two valence bands disappears from stoichiometric (111) to (110) surfaces. Similar phenomenon is also observed in the two PDOS plots for reduced surfaces. That is to say, the electron distribution in the (110) surface is denser and more continuous compared to that for (111) surface assuming the FM order along the [001] direction. For the stoichiometric (111) surface, we can see from calculated PDOS results that the U 5f orbital obviously hybridizes with O 2p orbital between approximate −5 and −1 eV, while the sharp and narrow peak within −1−0 eV is mainly assigned to be unpaired U 5f electron states. For the stoichiometric (110) surface, the electron density of U 5f and O 2p orbitals becomes slightly larger within a wider energy range below the Fermi energy. For reduced surfaces, the narrow peak around −2 eV becomes much higher and wider by comparison with the corresponding stoichiometric cases, because the valence electrons of uranium adjacent to the oxygen vacancy site are released partially from orbital hybridization. In Figure 2b,d, a minor component of U 5f peaks circled for clarity appears within the original band gap of

dx.doi.org/10.1021/jp503614f | J. Phys. Chem. C 2014, 118, 21935−21944

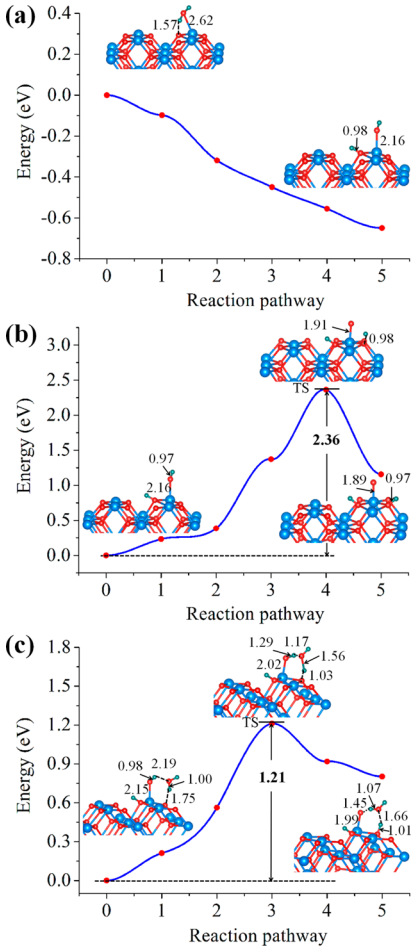

Figure 7. Calculated energy profiles for water dissociation: (a) first dehydrogenation, (b) second dehydrogenation, and (c) second dehydrogenation catalyzed by the water molecule on the stoichiometric (110) surface. The insets correspond to the optimized structures of the initial state (left), transition state (middle), and final state (right). The distance unit is Å. Color code as in Figure 3.

UO_2, which leads to the decrease of band gap of reduced surfaces significantly and also increases the surface activity. For the reduced (111) surface, the two excess electrons left from the missing surface oxygen atom are localized on the three U^{4+} ions next to the oxygen vacancy, which result to one U^{3+} ion and two $U^{(3+\delta)+}$ ions, respectively. However, for the reduced (110) surface, the two excess electrons are localized on the two U^{4+} ions next to the oxygen vacancy, forming two U^{3+} ions.

3.2. Molecular and Dissociative Adsorption of Water on Stoichiometric and Reduced (111) and (110) Surfaces. *3.2.1. Molecular Adsorption.* The interaction of uranium dioxide surfaces with water is of particular interest from mineralogical and nuclear waste management perspectives. Based on the above simulations, we further explored the molecular adsorption behavior of water on the relatively stable (111) and (110) surfaces of UO_2 crystal. In order to obtain stable adsorption structures of water on UO_2 surfaces, we carried out a series of AIMD simulations at 300 K starting with different initial atomic configurations of water molecule. The lowest energy structures obtained by these AIMD simulations are all selected for further DFT+U calculations to derive the local minimums on the potential energy surface of each adsorption system. The most stable adsorption geometries for a single water molecule on the stoichiometric (111) and (110) surfaces are respectively shown in Figure 3a,d. In these two cases, the oxygen atom of the adsorbed water molecule coordinates with a surface uranium atom, and one hydrogen atom of water coordinates with a neighboring surface oxygen atom. The obtained U−O(H_2) distances are 2.61 and 2.62 Å for the stoichiometric (111) and (110) surfaces, respectively. There are also hydrogen bonding between water and surface oxygen atom with the bond lengths of 1.61 and 1.57 Å for the stoichiometric (111) and (110) surface, respectively, which enhances the binding stability of the oxide surfaces. As listed in Table 2, the adsorption energies of a single water molecule are about −0.61 and −0.62 eV on the stoichiometric (111) and (110) surfaces, respectively. We can see that the stoichiometric (111) and (110) surfaces have almost the same adsorption energies for water. Recetnly, Maldonado et al.[9] also reported an adsorption energy of −1.10 eV for a single water molecule on the UO_2 (111) surface using LDA+U method. We can see the LDA+U method significantly overestimates the adsorption energy of molecular water on UO_2 surfaces with respect to the GGA+U method.

Turning now to the reduced surfaces, we have also carried out a series of AIMD simulations with different initial configurations to explore the probable adsorption structures of the water molecule. On the reduced (111) surface, we obtained two water adsorption configurations at given convergence criteria as shown in Figure 3b,c. In Figure 3b, the water molecule is adsorbed above a uranium site adjacent to the oxygen vacancy, forming one O−U bond of 2.66 Å and one hydrogen bond of 1.71 Å. The calculated adsorption energies are about −0.94 eV for this case. In Figure 3c, we find that the adsorbed water molecule locates above the oxygen vacancy after relaxation with the adsorption energy of −0.88 eV. On the reduced (110) surface, we only obtained one stable adsorption configuration of water molecule as shown in Figure 3e at given convergence criteria. In this case, the adsorbed water molecule also coordinates to the under-coordinated uranium atom via its oxygen terminal with the U−O(H_2) bond of about 2.64 Å. The calculated adsorption energy is about −1.42 eV on the reduced (110) surface. Our calculations show that the presence of the first layer oxygen vacancies increases the adsorption strength of water on low-index UO_2 surfaces here. One reason is that the under-coordinated U ions have more valence electrons available for bonding. When an oxygen atom is removed from the surface, the two excess electrons will be redistributed to the U^{4+} ions next to the oxygen vacancy, resulting in the reduction of these U^{4+} ions. The reduced U ions have higher chemical activity for reaction with adsorbates like water. Another reason is that, by removing an oxygen atom from the surface, the formed vacancy site tends to accommodate the oxygen ion of water and thus enhance the dissociation of O−H bonds.

3.2.2. Adsorption Stability of Partially Dissociative Water. Dissociation of water molecule adsorbed on the UO_2 surfaces will first dissociate into one hydroxyl radical and one hydrogen atom. In this section, we searched for relatively stable coadsorption structures of hydroxyl and hydrogen fragments on the stoichiometric UO_2 surfaces with the help of AIMD simulations. Some lowest energy structures were obtained along each AIMD trajectory and were selected for further DFT+U calculations. Figure 4a,c presents the optimized structures of partially dissociative water located on the stoichiometric surfaces. As expected, on the stoichiometric (111) and (110) surfaces, the hydroxyl radical coordinates with surface uranium

dx.doi.org/10.1021/jp503614f | J. Phys. Chem. C 2014, 118, 21935−21944

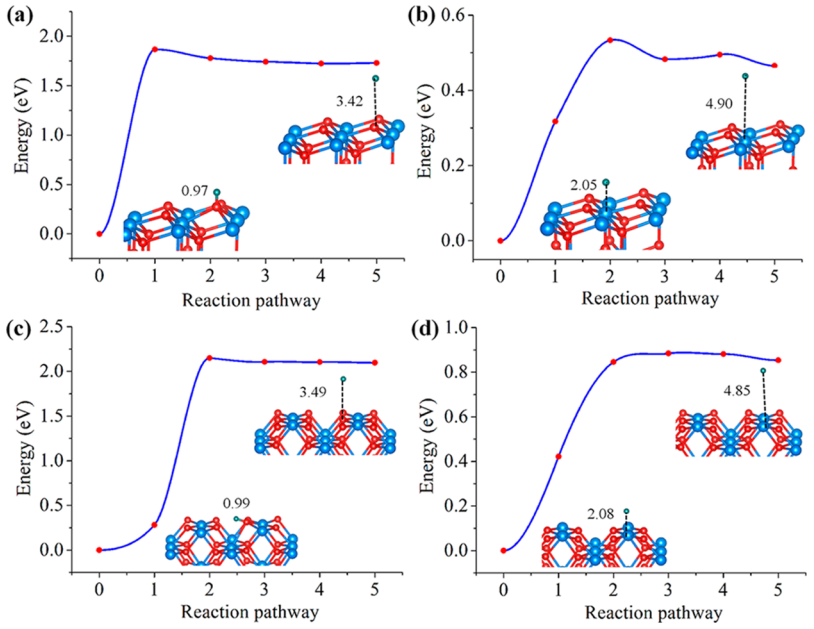

Figure 8. Calculated energy profiles for hydrogen abstraction from the stoichiometric (a) (111) surface oxygen atom, (b) (111) surface uranium atom, (c) (110) surface oxygen atom, and (d) (110) surface uranium atom. The insets correspond to the optimized structures of the initial state (left), and final state (right). The distance unit is Å. Color code as in Figure 3.

atom via its oxygen terminal, leaving the hydrogen atom from water bonded with a neighboring surface oxygen atom. On the stoichiometric (111) surface, the formed U−O(H) bond is about 2.24 Å, which is 0.37 Å shorter than the U−O(H_2) bond for molecular adsorption. On the stoichiometric (110) surface, the calculated U−O(H) distance for the adsorbed hydroxyl radical is about 2.16 Å, which is 0.46 Å shorter than the corresponding U−O(H_2) in molecular adsorption case. The calculated adsorption energies of partially dissociative water are about −0.68 and −1.27 eV for stoichiometric (111) and (110) surfaces, respectively (see Table 2). We can see the partially dissociative adsorption energy for water is about twice as much as the molecular adsorption energy on the stoichiometric (110) surface. Maldonado et al.[9] reported that the adsorption energy for dissociative water is −1.12 eV on the UO_2 (111) surface using the LDA+U method, very similar to the energy of molecular adsorption (−1.10 eV). This phenomenon agrees well with our GGA+U calculations (−0.61 vs −0.68 eV). Rák et al.[8] reported energies of −0.29 and −1.05 eV for dissociative adsorption of a single water on the UO_2 (111) and (110) surfaces using the GGA+U method, respectively, which are obviously smaller than our results. These differences are probably due to the use of the small (1 × 1) slabs in their work, and thus the repulsive interaction between hydroxyl ions was strengthened.

Actually, the adsorption behaviors of water can be affected by water molecules preexisting on the surface. As the water coverage increases, the efficient H-bonds between water molecules will be formed which can strengthen the adsorption stability. However, high water coverage can lead to high repulsive interaction between neighboring water molecules, which can weaken the adsorption stability to different extents.[9] The main objective of this paper is to study the single water adsorption on the stoichiometric and reduced UO_2 surfaces and the formation mechanisms of H_2 on the reduced (111) surface. The coverage dependence for water adsorption on the UO_2 surfaces will be thoroughly discussed in another work in the future.

As for the reduced UO_2 surfaces, we simulated the adsorption of the partially dissociative water on the (111) and (110) surfaces in the presence of a first layer oxygen vacancy. As shown in Figure 4b, the most stable partially dissociative adsorption configuration of water on reduced (111) surface is characterized by location of the oxygen atom of the hydroxyl radical above an oxygen vacancy and bonding of the left hydrogen atom with the neighboring surface oxygen atom. The obtained adsorption energy for this partial dissociation case reaches about −2.20 eV. In addition, we obtained two adsorption configurations for partially dissociative water on the reduced (110) surface as exhibited in Figure 4d,e, in both of which the hydroxyl ion prefers to lie on the oxygen vacancy. The adsorption energy for the most stable adsorption configuration in Figure 4d is about −2.11 eV, which is slightly higher than −1.78 eV for the configuration in Figure 4e, owing to the presence of a hydrogen bond in the former case. We can deduce that the presence of an oxygen vacancy significantly enhances the binding strength of the partially dissociative water with UO_2 surfaces.

3.2.3. Adsorption Stability of Completely Dissociative Water. In this section, we further explored the adsorption behavior of completely decomposed water molecule. For simplification we just considered the stoichiometric UO_2 (111) and (110) surface here. Figure 5 shows the optimized adsorption structures of the completely dissociative water, producing two hydrogen atoms and one oxygen atom on UO_2 surfaces. We can see the hydrogen atoms bond with two surface oxygen atoms, while the oxygen atom from water is bonded to the uranium atom, as expected. The calculated adsorption energies of the completely dissociative water are +0.15 and −0.11 eV on the stoichiometric UO_2 (111) and (110) surfaces, respectively. Such high adsorption energies suggest reactions of complete water dissociation with no significant energy release or absorption.

dx.doi.org/10.1021/jp503614f | J. Phys. Chem. C 2014, 118, 21935−21944

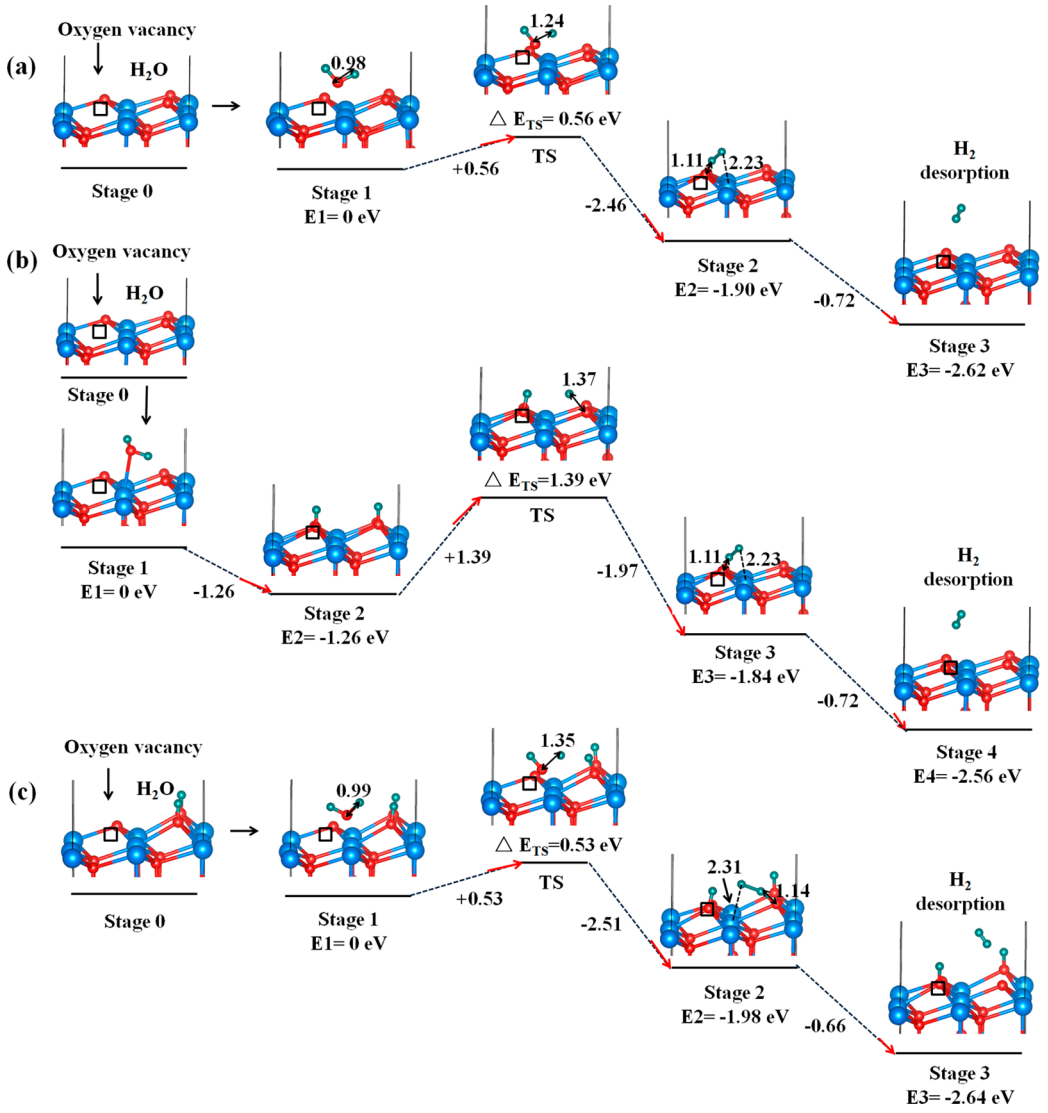

Figure 9. Calculated energy landscapes for three H_2 formation and desorption pathways on the reduced UO_2 (111) surface. Color code as in Figure 3. The black boxes denote oxygen vacancies. ΔE_{TS} is the energy of the TS relative to the previous state. The distance unit is Å. The energy unit is eV.

3.2.4. Minimum Energy Reaction Path for Water Dissociation. In this section we systematically investigated the probable stepwise dissociation pathways of the water molecule on the stoichiometric UO_2 (111) surface. The minimum energy path for water dissociation was modeled by the climbing image NEB method.[31−33] The initial and final configurations for each dissociation reaction come from the derived most stable adsorption structures of molecular and dissociative water on the stoichiometric UO_2 (111) surface, respectively. The relative energies of the initial, transition, and final states and the corresponding structures are illustrated in Figure 6.

Figure 6a exhibits the calculated reaction pathway of the first dehydrogenation process of the water molecule on the stoichiometric UO_2 (111) surface. Based on our calculations, abstraction of the first H atom from water molecule adsorbed on top of the uranium site just needs to overcome one energy barrier of about 0.13 eV. At the transition state, the interaction distances from the dissociating H atom to the oxygen atom of water and the nearest surface oxygen atom are 1.18 and 1.27 Å, respectively. This means that the molecular water can readily dissociate to one hydroxyl radical and one hydrogen atom on the stoichiometric UO_2 (111) surface.

We next investigated the second dehydrogenation process of the water molecule on the stoichiometric UO_2 (111) surface, where the remaining OH radical dissociates into H and O. As shown in Figure 6b, the initial configuration is the one with the hydroxyl radical bound to one surface uranium atom and the dissociated hydrogen atom bound to the nearest surface oxygen atom. At the transition state, the OH bond is stretched from 0.97 to 1.43 Å, and the dissociating H atom extends toward a neighboring surface oxygen atom. In the final configuration, both hydrogen atoms from water are captured on top of surface oxygen atoms, forming two hydroxyl radicals, while the oxygen atom from water stays on top of the uranium atom. This dissociation process is strongly endothermic by about 0.77 eV and has a large energy barrier of about 0.92 eV, suggesting that direct dissociation of the OH group on the UO_2 (111) surface is energetically unfavorable.

Some previous experimental and theoretical studies[34,35] have studied the behavior of water dissociative adsorption on the Fe_3O_4 (111) surface. The dissociation reactions of the water molecule and the hydroxyl radical can be readily catalyzed by

dx.doi.org/10.1021/jp503614f | J. Phys. Chem. C 2014, 118, 21935−21944

water molecules around the active sites. Considering the obtained large energy barrier for hydroxyl dissociation, we further investigated the hydroxyl dissociation reaction catalyzed by another water molecule on the UO_2 (111) surface. As shown in Figure 6c, in the initial configuration, another water molecule is adsorbed adjacent to one hydroxyl radical on the UO_2 (111) surface, forming hydrogen bonds with the H atom of the hydroxyl radical and the surface oxygen atom simultaneously. In the transition state, the hydrogen bond between the H atom of the hydroxyl radical and the oxygen atom of the water molecule significantly contracts from 1.92 to 1.10 Å, accompanying with the stretching of the downward O−H bond of water from 0.99 to 1.40 Å. The dissociated hydrogen atom from the water molecule is transferred toward the nearest surface oxygen atom. In the final configuration, the hydroxyl radical dissociates via the aid of another water molecule completely. The total process is calculated to be endothermic by 0.55 eV and has an energy barrier of 0.70 eV, which is obviously lower than the value of 0.92 eV without water catalysis. This suggests that the presence of a water molecule can help to reduce the energy barrier for hydroxyl dissociation.

The minimum energy paths for water dissociation and the catalytic effect of water molecule were also investigated on the stoichiometric UO_2 (110) surface. For dissociation of water molecule into hydroxyl radical, as shown in Figure 7a, the initial and final configurations were similar to those on the stoichiometric (111) surface mentioned above. This dissociation process is exothermic by −0.65 eV and is totally barrierless, which means that dissociative water adsorption is more preferable than molecular adsorption on the stoichiometric (110). The reaction pathway for further dissociation of the remaining OH fragment is shown in Figure 7b. This dissociation process is strongly endothermic by 1.16 eV and has a larger energy barrier of 2.36 eV, which is about twice as much as that on the stoichiometric (111) surface (0.92 eV). The catalysis effect of the H_2O molecule on OH dissociation on the UO_2 (110) surface has also been probed. As shown in Figure 7c, this reaction process occurs by simultaneous transfer of one hydrogen atom from the hydroxyl to the water molecule and from the water molecule to the surface oxygen atom. The dissociation of the second H atom of water is endothermic by 0.8 eV on the UO_2 (110) surface, smaller than that without water catalysis (1.16 eV). The water catalysis decreases the obtained energy barrier of hydroxyl dissociation to 1.21 eV significantly, compared with the value of 2.36 eV without water catalysis.

3.3. H_2 Formation and Desorption on Reduced (111) Surfaces. Upon the dissociation of water molecules on the reduced UO_2 surfaces, a series of reactions are possible leading to the release of H_2 molecules, as indicated by Senanayake et al.[16] and Stulz et al.[36] It is important to understand these reactions because the formation of H_2 is dangerous for the storage of spent fuel. In this part, we have studied the reaction mechanisms leading to H_2 formation.

3.3.1. Adsorption and Desorption of H Atom. Before H_2 formation on the UO_2 (111) surface, the dissociated H atom is mainly captured by the surface oxygen as discussed above. From our calculations, the adsorption energy of a single H atom is −1.73 eV on top of the oxygen atom on the stoichiometric UO_2 (111) surface but is just −0.46 eV above the uranium atom. The calculated O−H and U−H bonds are 0.97 and 2.05 Å, respectively. In contrast, on the stoichiometric UO_2 (110) surface, the adsorption energies of the H atom are −2.10 and −0.85 eV on the oxygen and uranium atoms, respectively. The O−H and U−H bonds become 0.99 and 2.08 Å, respectively. That is to say, the H atom prefers to be captured by the surface oxygen atom prior to the uranium atom. The abstraction pathway of the chemisorbed H atom from UO_2 surfaces has been investigated as shown in Figure 8. Here, we obtained the final states by moving the adsorbed H atom far away from the surface and then performing optimization. From our calculations, the abstraction of the H atom from UO_2 (111) and (110) surfaces needs to overcome an energy barrier comparable to its adsorption energy, and the whole process is significantly endothermic. Please see the details about H adsorption and abstraction on UO_2 surfaces in the Supporting Information.

3.3.2. Reactions Pathways of H_2 Formation. Based on the above results, we explored the probable reaction mechanisms for H_2 formation on the stable UO_2 (111) surface. Figure 9 shows the obtained three formation pathways on the reduced UO_2 (111) surface derived from our first-principles calculations. The first H_2 formation pathway is shown in Figure 9a. In this case, once a water molecule is adsorbed above a surface oxygen vacancy (stage 1), one of its hydrogen atoms breaks away from the oxygen center of water and binds to the other hydrogen atom directly, thus forming the surface O−H−H structure which directs to the neighboring uranium atom with the U−H distance of 2.23 Å (stage 2). At the obtained transition state the interaction distance between the dissociating H atom and the oxygen atom of water molecule is enlongated to be 1.24 Å. This process has an energy barrier of 0.56 eV and is largely exothermic by −1.90 eV. The final step is the release of the H_2 molecule from the surface, which is exothermic by −0.72 eV. Therefore, the overall H_2 formation pathway in case (a) is exothermic by −2.62 eV relative to stage 1 and presents an energy barrier of 0.56 eV. The second H_2 formation pathway is shown in Figure 9b. In this case, the water molecule adsorbed on top of the surface uranium atom dissociates into one hydroxyl radical and one hydrogen atom as shown in stage 2, with the hydroxyl radical occupying the oxygen vacancy and the hydrogen atom bonding to the surface oxygen atom. The first dehydrogenation process is exothermic by −1.26 eV and barrierless. In the next step, one hydrogen atom breaks away from the oxygen atom and moves toward the other hydrogen atom to form an O−H−H structure as mentioned above (stage 3). This reaction process (from stage 2 to stage 3) has a high energy barrier of 1.39 eV and the reaction energy of −0.58 eV. The final step is desorption of the formed H_2 molecule with no energy barrier, which is exothermic by −0.72 eV. Therefore, the overall H_2 formation pathway in the second case is also exothermic by −2.56 eV relative to stage 1 and presents a larger energy barrier of 1.39 eV. The third H_2 formation pathway is provided in Figure 9c, in which excess hydrogen atoms are adsorbed adjacent to the surface reactive site (stage 0). The key step of this process is the breaking of one H−O bond of water molecule adsorbed on top of the oxygen vacancy (TS) and the following bonding between the dissociating H atom and another H atom on the surface (stage 2). At the obtained transition state, the interaction distance between the dissociating H atom and the oxygen atom of water molecule is enlongated from 0.99 to 1.35 Å. This process is exothermic by −1.98 eV and has an energy barrier of 0.53 eV, which is close to that for the first pathway. The desorption of the H_2 molecule in the final step remains exothermic by −0.66 eV. The third H_2 formation pathway is

ultimately exothermic by −2.64 eV and has an energy barrier of 0.53 eV.

Based on the above discussion, all the derived reaction paths for H_2 formation and desorption obtained here are highly exothermic (>2.5 eV). By comparison, we find that the first and the third H_2 formation pathways are more favorable with lower activation barriers of about 0.56 and 0.53 eV on the reduced UO_2 (111) surface, respectively. In contrast, the second path is with an energy barrier as high as 1.39 eV, inhibited by the break of one stable surface O−H bond in the transition state. These results are helpful for further understanding the reaction mechanisms leading to H_2 formation on the reduced UO_2 (111) surface.

4. CONCLUSIONS

In this work, we studied the adsorption and dissociation behaviors of water as well as the following hydrogen formation processes on the stoichiometric and reduced (111) and (110) surfaces of UO_2 crystal by using DFT+U calculations. From our calculations, the calculated surface energies for the (111) and (110) surfaces are 0.73 and 1.06 J/m^2, respectively. The higher stability of the (111) surface leads to higher defect formation energy compared to the (110) surface. The obtained formation energies of oxygen vacancy in the first oxygen layer reach 5.95 and 5.38 eV for the (111) and (110) surfaces, respectively, which are slightly lower than that for bulk UO_2 (6.14 eV). The calculated electronic density of states indicates that the introduction of surface oxygen vacancy significantly decreases the band gap of these UO_2 surfaces and correspondingly increases the surface activity.

Our detailed study reveals that, on the stoichiometric (111) surface, the water molecule adsorbed atop the uranium atom can readily dissociate into a hydroxyl group by first dehydrogenation, leaving the dissociated hydrogen atom bounded to the adjacent oxygen atom. The obtained energy barrier for the first dehydrogenation reaction is only 0.13 eV. In contrast, the key step of water dissociation becomes the second dehydrogenation process, for which the energy barrier reaches about 0.92 eV, respectively. The catalysis capability of the water molecule to its neighbor was confirmed, and the water-catalyzed second dehydrogenation process of the water molecule has an energy barrier of 0.70 eV. The second dehydrogenation process is endothermic by 0.77 and 0.55 eV with noncatalysis and water-catalysis, respectively. On the (110) stoichiometric surface, the first dehydrogenation of the water molecule is barrierless and exothermic by −0.65 eV. Compared to the stoichiometric (111) surface, the second dehydrogenation process is still a key step on the (110) stoichiometric surface, while the energy barrier significantly increases to 2.36 and 1.21 eV with noncatalysis and water-catalysis, respectively. The second dehydrogenation process is endothermic by 1.16 and 0.8 eV for the above two cases, respectively.

According to our calculations, the H_2 formation after water dissociation can undergo different pathways on the reduced UO_2 (111) surface. One probable pathway is characterized by the direct combination of two hydrogen atoms of the water molecule and the formation of an intermediate with the linear O−H−H structure on the surface. The other pathway is characterized by dissociation of the first hydrogen atom of water and its combination with a neighboring surface hydrogen atom. The above two formation pathways possess the energy barriers of 0.56 and 0.53 eV corresponding to the reaction energies of −2.62 and −2.64 eV, respectively. This work can aid in understanding the adsorption and dissociation behaviors of a water molecule on the stoichiometric UO_2 surfaces and the following H_2 formation mechanism.

■ ASSOCIATED CONTENT

Ⓢ Supporting Information

Adsorption of H atom on the stoichiometric UO_2 (111) and (110) surfaces, and abstraction of H atom on the stoichiometric UO_2 (111) and (110) surfaces. This material is available free of charge via the Internet at http://pubs.acs.org.

■ AUTHOR INFORMATION

Corresponding Authors

*E-mail: shiwq@ihep.ac.cn.
*E-mail: zfchai@suda.edu.cn.

Author Contributions

The first two authors contributed equally to this work.

Notes

The authors declare no competing financial interest.

■ ACKNOWLEDGMENTS

This work was supported by the National Natural Science Foundation of China (Grant Nos. 91326202, 91126006, 21201166, and 21101157) and the "Strategic Priority Research Program" of the Chinese Academy of Sciences (Grant No. XDA030104).

■ REFERENCES

(1) Fanganel, T.; Rondinella, V. V.; Glatz, J. P.; Wiss, T.; Wegen, D. H.; Gouder, T.; Carbol, P.; Serrano-Purroy, D.; Papaioannou, D. Reducing Uncertainties Affecting the Assessment of the Long-Term Corrosion Behavior of Spent Nuclear Fuel. *Inorg. Chem.* **2013**, *52*, 3491−3509.

(2) Senanayake, S. D.; Waterhouse, G. I. N.; Chan, A. S. Y.; Madey, T. E.; Mullins, D. R.; Idriss, H. The Reactions of Water Vapour on the Surfaces of Stoichiometric and Reduced Uranium Dioxide: A High Resolution Xps Study. *Catal. Today* **2007**, *120*, 151−157.

(3) Wen, X. D.; Martin, R. L.; Henderson, T. M.; Scuseria, G. E. Density Functional Theory Studies of the Electronic Structure of Solid State Actinide Oxides. *Chem. Rev.* **2013**, *113*, 1063−1096.

(4) Skomurski, F. N.; Shuller, L. C.; Ewing, R. C.; Becker, U. Corrosion of UO_2 and ThO_2: A Quantum-Mechanical Investigation. *J. Nucl. Mater.* **2008**, *375*, 290−310.

(5) Dorado, B.; Amadon, B.; Freyss, M.; Bertolus, M., DFT+U Calculations of the Ground State and Metastable States of Uranium Dioxide. *Phys. Rev. B* **2009**, *79*.

(6) Lan, J.-H.; Wang, L.; Li, S.; Yuan, L.-Y.; Feng, Y.-X.; Sun, W.; Zhao, Y.-L.; Chai, Z.-F.; Shi, W.-Q., First Principles Modeling of Zirconium Solution in Bulk UO_2. *J. Appl. Phys.* **2013**, *113*.

(7) Lan, J.-H.; Zhao, Z.-C.; Wu, Q.; Zhao, Y.-L.; Chai, Z.-F.; Shi, W.-Q. First-Principles DFT+U Modeling of Defect Behaviors in Anti-Ferromagnetic Uranium Mononitride. *J. Appl. Phys.* **2013**, *114*, 223516.

(8) Rák, Z.; Ewing, R. C.; Becker, U. Hydroxylation-Induced Surface Stability of AnO_2 (An=U, Np, Pu) from First-Principles. *Surf. Sci.* **2013**, *608*, 180−187.

(9) Maldonado, P.; Evins, L. Z.; Oppeneer, P. M. *Ab Initio* atomistic Thermodynamics of Water Reacting with Uranium Dioxide Surfaces. *J. Phys. Chem. C* **2014**, *118*, 8491−8500.

(10) Wang, J.; Ewing, R. C.; Becker, U., Electronic Structure and Stability of Hyperstoichiometric UO_{2+X} under Pressure. *Phys. Rev. B* **2013**, *88*.

(11) Boettger, J. C.; Ray, A. K. Fully Relativistic Density Functional Calculations on Hydroxylated Actinide Oxide Surfaces. *Int. J. Quantum Chem.* **2002**, *90*, 1470−1477.
(12) Skomurski, F. N.; Ewing, R. C.; Rohl, A. L.; Gale, J. D.; Becker, U. Quantum Mechanical Vs. Empirical Potential Modeling of Uranium Dioxide (UO_2) Surfaces: (111), (110), and (100). *Am. Mineral.* **2006**, *91*, 1761−1772.
(13) Alexandrov, V.; Shvareva, T. Y.; Hayun, S.; Asta, M.; Navrotsky, A. Actinide Dioxides in Water: Interactions at the Interface. *J. Phys. Chem. Lett.* **2011**, *2*, 3130−3134.
(14) Jomard, G.; Bottin, F., Thermodynamic Stability of PuO_2 Surfaces: Influence of Electronic Correlations. *Phys. Rev. B* **2011**, *84*.
(15) Sun, B.; Liu, H.; Song, H.; Zhang, G.; Zheng, H.; Zhao, X.; Zhang, P. First-Principles Study of Surface Properties of PuO_2: Effects of Thickness and O-Vacancy on Surface Stability and Chemical Activity. *J. Nucl. Mater.* **2012**, *426*, 139−147.
(16) Senanayake, S. D.; Idriss, H. Water Reactions over Stoichiometric and Reduced UO_2 (111) Single Crystal Surfaces. *Surf. Sci.* **2004**, *563*, 135−144.
(17) LaVerne, J. A.; Tandon, L. H_2 Production in the Radiolysis of Water on UO_2 and Other Oxides. *J. Phys. Chem. B* **2003**, *107*, 13623−13628.
(18) Jonsson, M.; Nielsen, F.; Roth, O.; Ekeroth, E.; Nilsson, S.; Hossain, M. M. Radiation Induced Spent Nuclear Fuel Dissolution under Deep Repository Conditions. *Environ. Sci. Technol.* **2007**, *41*, 7087−7093.
(19) Abramowski, M.; Redfern, S. E.; Grimes, R. W.; Owens, S. Modification of UO_2 Crystal Morphologies through Hydroxylation. *Surf. Sci.* **2001**, *490*, 415−420.
(20) Tan, A. H. H.; Grimes, R. W.; Owens, S. Structures of UO_2 and PuO_2 Surfaces with Hydroxide Coverage. *J. Nucl. Mater.* **2005**, *344*, 13−16.
(21) Kresse, G.; Hafner, J. Ab initio Molecular Dynamics for Liquid Metals. *Phys. Rev. B* **1993**, *47*, 558−561.
(22) Kresse, G.; Furthmuller, J. Efficiency of ab-initio Total Energy Calculations for Metals and Semiconductors Using a Plane-Wave Basis Set. *Comput. Mater. Sci.* **1996**, *6*, 15−50.
(23) Kresse, G.; Furthmüller, J. Efficient Iterative Schemes for *ab initio* Total-Energy Calculations Using a Plane-Wave Basis Set. *Phys. Rev. B* **1996**, *54*, 11169−11186.
(24) Blöchl, P. E. Projector Augmented-Wave Method. *Phys. Rev. B* **1994**, *50*, 17953−17979.
(25) Kresse, G.; Joubert, D. From Ultrasoft Pseudopotentials to the Projector Augmented-Wave Method. *Phys. Rev. B* **1999**, *59*, 1758−1775.
(26) Perdew, J. P.; Burke, K.; Ernzerhof, M. Generalized Gradient Approximation Made Simple. *Phys. Rev. Lett.* **1996**, *77*, 3865−3868.
(27) Monkhorst, H. J.; Pack, J. D. Special Points for Brillouin-Zone Integrations. *Phys. Rev. B* **1976**, *13*, 5188−5192.
(28) Idiri, M.; Le Bihan, T.; Heathman, S.; Rebizant, J., Behavior of Actinide Dioxides under Pressure:UO_2 and ThO_2. *Phys. Rev. B* **2004**, *70*.
(29) Prodan, I. D.; Scuseria, G. E.; Sordo, J. A.; Kudin, K. N.; Martin, R. L. Lattice Defects and Magnetic Ordering in Plutonium Oxides: A Hybrid Density-Functional-Theory Study of Strongly Correlated Materials. *J. Chem. Phys.* **2005**, *123*, 014703.
(30) Jomard, G.; Amadon, B.; Bottin, F.; Torrent, M., Structural, Thermodynamic, and Electronic Properties of Plutonium Oxides from First Principles. *Phys. Rev. B* **2008**, *78*.
(31) Henkelman, G.; Jonsson, H. Theoretical Calculations of Dissociative Adsorption of CH_4 on an Ir(111) Surface. *Phys. Rev. Lett.* **2001**, *86*, 664−667.
(32) Henkelman, G.; Uberuaga, B. P.; Jonsson, H. A Climbing Image Nudged Elastic Band Method for Finding Saddle Points and Minimum Energy Paths. *J. Chem. Phys.* **2000**, *113*, 9901−9904.
(33) Henkelman, G.; Jonsson, H. Improved Tangent Estimate in the Nudged Elastic Band Method for Finding Minimum Energy Paths and Saddle Points. *J. Chem. Phys.* **2000**, *113*, 9978−9985.
(34) Cutting, R. S.; Muryn, C. A.; Vaughan, D. J.; Thornton, G. Substrate-Termination and H_2O-Coverage Dependent Dissociation of H_2O on Fe_3O_4(111). *Surf. Sci.* **2008**, *602*, 1155−1165.
(35) Zhou, C. G.; Zhang, Q. F.; Chen, L.; Han, B.; Ni, G.; Wu, J. P.; Garg, D.; Cheng, H. S. Density Functional Theory Study of Water Dissociative Chemisorption on the Fe_3O_4(111) Surface. *J. Phys. Chem. C* **2010**, *114*, 21405−21410.
(36) Stultz, J.; Paffett, M. T.; Joyce, S. A. Thermal Evolution of Hydrogen Following Water Adsorption on Defective UO_2(100). *J. Phys. Chem. B* **2004**, *108*, 2362−2364.